ISSN 1995-4239, Numerical Analysis and Applications, 2019, Vol. 12, No. 3, pp. 219–233. © Pleiades Publishing, Ltd., 2019.
Russian Text © The Author(s), 2019, published in Sibirskii Zhurnal Vychislitel'noi Matematiki, 2019, Vol. 22, No. 3, pp. 259–276.

Simulation of Body Motion in Viscous Incompressible Fluid

A. S. Kozelkov[1,2*], V. R. Efremov[3], A. A. Kurkin[2***], N. V. Tarasova[1****], D. A. Utkin[1*****], and E. S. Tyatyushkina[2******]**

[1] *All-Russian Research Institute of Experimental Physics of the Russian Federal Nuclear Center, pr. Mira 37, Nizhegorodskaya oblast, Sarov, 607188 Russia*

[2] *Alekseev Nizhny Novgorod State Technical University, ul. Minina 24, Nizhny Novgorod, 603950 Russia*

[3] *Shipunov Instrument Design Bureau, ul. Shcheglovskaya Zaseka 59, Tula, 300001 Russia*

Received April 3, 2018; in final form, September 4, 2018; accepted May 7, 2019

Abstract—The paper presents a description of a method for simulation of the motion of bodies in viscous incompressible fluid with the use of a technique of computation on overset grids ("chimera" technique). Equations describing the flow of viscous incompressible fluid are approximated by the finite volume method on an arbitrary unstructured grid. Their iterative solution is implemented using the algorithm SIMPLE. This paper describes the basic equations in the case of moving grid. The features of implementation of grid boundary conditions that are set in the course of construction of interpolation pattern are described. A method for overcoming numerical instability when a solid body model is used is demonstrated. The specificity of taking into account the forces of gravitation in the presence of multiphase media is described. The results of solving the problem of motion of cylinder in fluid, fall of sphere into fluid, and flooding of a ship's model are presented.

DOI: 10.1134/S1995423919030029

Keywords: *chimera technique, method SIMPLE, unstructured grid, multiphaseness, solid body.*

1. INTRODUCTION

At present, in computational fluid dynamics there is a large class of practical problems related to motion of bodies in an incompressible fluid. These include movement of particles in branched channels or vessels [1] and chemical reactors, movement and flooding of ships in water [2], flows with deformation of boundaries [3], simulation of flow in a mixer, simulation of departure of torpedoes into a liquid medium, and so on. Many problems of practical use relate to simulation of non-stationary three-dimensional processes that take into account the motion of objects relative to each other.

At present, motion of bodies in fluid is modeled using the methods of adaptable grids [4], moving grids [5], immersed boundaries [6], and grid embedding [7] ("chimera" grids).

The use of the technique of adaptively embedded grids implies the generation of a new computational grid, corresponding to the current position of the boundaries, for each moment of time. This approach has a disadvantage of high computational cost—the process of grid building at each computational step significantly exceeds the execution time of the iterative procedure of the numerical method. This time may differ tenfold, especially when the grid is built in regions of complex geometric configuration. The use of moving grids with the preservation of the grid topology instead of building a new grid only changes the position of the nodes, which can significantly reduce the rebuilding time. However, if strong deformations are taken into account, the quality of the resulting grid can be unsatisfactory and the probability of

*E-mail: askozelkov@mail.ru
**E-mail: valentin_e@mail.ru
***E-mail: aakurkin@gmail.com
****E-mail: tara@vniief.ru
*****E-mail: dimitryavich@yandex.ru
******E-mail: Leno4ka-07@mail.ru

formation of highly distorted cells is high. Therefore, this approach is used only if the relative motion of objects is insignificant. The method of immersed boundaries is attractive because it enables calculations on Cartesian grids with a higher order of approximation. Its disadvantages include the low accuracy of prediction of friction force, necessity of impenetrability condition, and the process of reconstruction of boundaries of the solid [8].

One of the options that combine the merits of the computational methods on adaptively embedded and moving grids is the technology of computation on overset grids [7, 9]. This approach implies construction of independent grids for individual elements of the computational domain with subsequent merging of the grids into one common mesh with overlapping regions (the so-called chimera technique). Each grid takes into account the shape and geometrical features of its element only, which enables significant simplification of the process of building a common computational mesh for a common domain of complex geometric configuration. Most works on overset grids are associated with studying the accuracy of interpolation algorithms [10, 11] and construction of conservative calculation schemes [12, 13]. Initially, the chimera method was developed for structured meshes. The possibility of adapting the chimera method for computation on arbitrary unstructured grids [14] creates tremendous potential for successfully solving many practical problems [15–17]. The use of such symbiosis can significantly reduce the calculation time, simplify the procedure for constructing a computational mesh in domains of complex geometric configuration, and reduce the computational load.

From analysis of the literature, it follows that the use of such an approach together with the finite volume method has not yet become widespread [16–19]. Moreover, even fewer works deal with the use of unstructured overset grids for solving practical problems associated with the motion of bodies in viscous incompressible fluid.

When developing technology for motion of bodies in viscous incompressible fluid, in addition to consistent determination of velocity and pressure fields (SIMPLE-type algorithms) [20], it is necessary to take into account details of implementation of interpolation algorithms on grid interfaces and computation of discontinuous density field in simulation of a free-surface flow in the gravity field.

This paper presents a method for calculating the motion of bodies in viscous incompressible fluid based on the chimera technique. The equations describing the flow of viscous non-compressible fluid are approximated using the finite volume method on an arbitrary unstructured mesh. The iterative procedure for solving the problem is based on the algorithm SIMPLE. The paper presents the basic equations of the method and their modification for the general case of grid movement, and also describes the features of realization of conditions at the boundaries of the grid regions, which are set in the course of construction of an interpolation pattern using the chimera technique. Particularities of modeling of motion of bodies in a multiphase medium are indicated. A method for overcoming numerical instability when a solid body model is used is described.

The efficiency of the presented method is demonstrated by the example of solving several problems: movement of cylinder in fluid, ball falling into fluid, and flooding of model of damaged ship.

2. COMPUTATION METHODS

2.1. Overset Grid Method

The key features of the overset grid method (the chimera method) are discussed in [7]. Research in the field of computation on overset grids is mostly devoted to structured grids. In [19], the stages of construction of computation technique on unstructured overset grids, which can be used with grids of arbitrary polyhedra with non-planar faces, are described, as well as the basic algorithms required for constructing an interpolation pattern to ensure interaction of topologically unbound regions.

The main stages of preparing a computational model, including the generation of geometric models, merge of models, and construction of an interpolation pattern, will be demonstrated by the example of a computational mesh for the problem of cylinder moving in fluid.

The computational model is created with the construction of two independent computational grids: one for the entire external modeling domain and the other in the vicinity of the moving body (cylinder) (Fig. 1). Further, these grids are combined into one computational model consisting of two overset grids.

An interpolation pattern is built for this model. Construction of such a pattern implies determination of computational and non-computational cells, generation of new internal boundary conditions, and formation of donor and acceptor cells (Fig. 2). The new boundaries created in the course of constructing

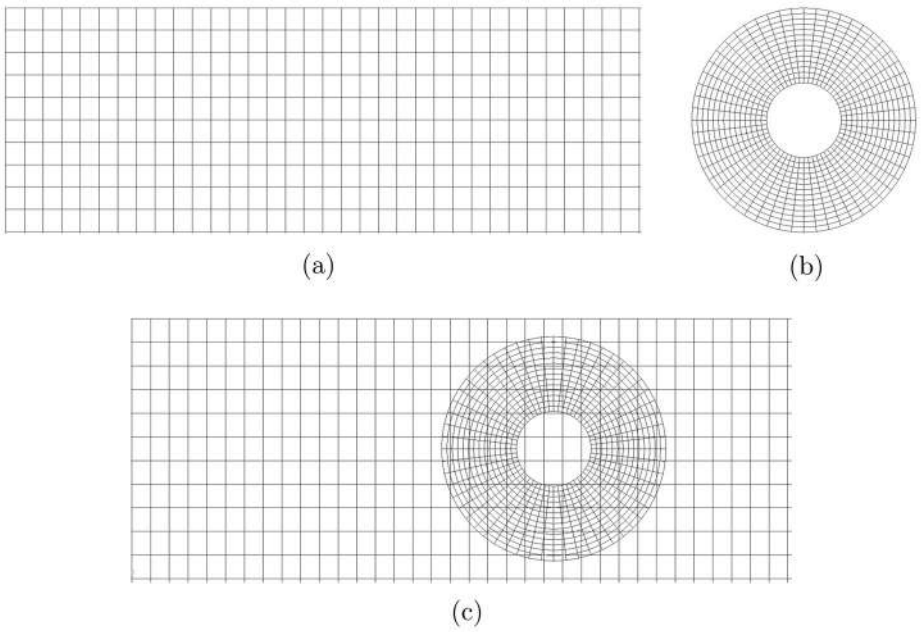

Fig. 1. Computational grid: (a) computational grid of external region; (b) grid around body; (c) resulting mesh with overlappings.

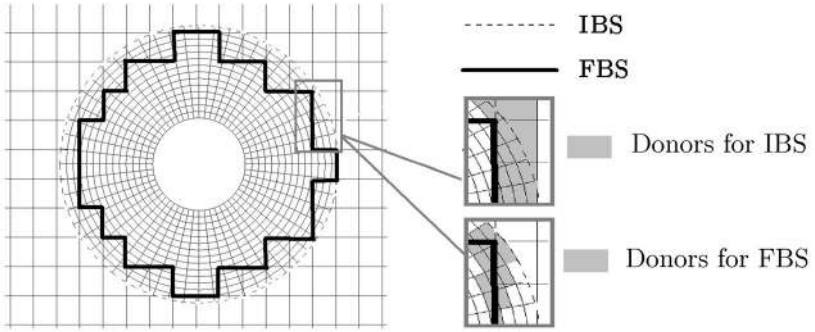

Fig. 2. Interpolation pattern.

the pattern and marking the cells of the common mesh are called the Fringe Boundary Surface (FBS). Along with the open boundaries of the Interpolation Boundary Surface (IBS), they provide communication interaction of bound regions and form the required initial data of the interpolation pattern [7, 19].

The IBS boundary is the outer boundary of one of the regions; all the faces of the boundary are acceptors. The FBS is the set of the acceptor faces of one of the regions, which separate computational cells from those declared non-computational for a given moment and form a new boundary. A donor is a cell that is computational for one of the grid regions and whose computation data can be used for interpolation of values to acceptor faces belonging to another grid region. For each acceptor face, there are computational cells from other regions on the basis of which the parameters at the boundary are reconstructed (Fig. 2). Thus, construction of the pattern yields a new class of boundary conditions of the "interface" type (FBS/IBS), and this class ensures interaction of grids that are topologically uncoupled with each other.

Using the method of overset grids in conjunction with various algorithms for solving problems of aerohydrodynamics and heat transfer implies development of special approaches for processing interface faces. Viscous incompressible flows are modeled using the segregated algorithm SIMPLE

[20]. In this case, the Navier–Stokes system of equations is solved sequentially, the splitting into the physical processes taken into account. First, the equation for calculating the velocity field is solved with application of the predictor–corrector procedure, and then the pressure field is found. In the case of finite volume discretization, all the values are stored in the centers of control volumes, and computation of convective flows involves approximation of the values on the boundary of the computational grid.

In processing interface faces, it is necessary to take into account the fact that they are essentially internal faces, although interpolated calculated data from donor cells are already stored on them as on acceptor faces. In this connection, the following algorithm is proposed.

Let us take a face with the index f, belonging to the FBS (IBS). Let $\varphi_f(\varphi \in \{u, v, w, p, \rho, \dots\})$ be the values of computational quantities on the f face, interpolated from donor cells, F_f be the flow through the face f, φ_k be the values of the quantities in the center of the cell with the index k adjacent to the face with the index f, and $\tilde{\varphi}_f$ be the resulting values of the quantities on the face f.

1. In discretization of the momentum conservation equation at the predictor stage, the value of the fields on the interface faces is determined as the arithmetic average of the values obtained from the donor cells and from the center of the adjacent cell: $\tilde{\varphi}_f = 0.5(\varphi_f + \varphi_k)$. The use of such averaging is analogous to the central difference scheme when the geometric factor is unknown.

2. When the equation for pressure at the corrector stage is solved, an acceptor face is considered as an external boundary and the computational fields on it are reconstructed depending on the flow direction:

   (a) at $F_f < 0$ (inflow) $\tilde{\varphi}_f = \varphi_f$ for $\varphi \in \{u, v, w, \rho\}$, $\tilde{p}_f = p_k$;

   (b) at $F_f > 0$ (the flow is directed from the computational cell adjacent to this face), on the contrary, $\tilde{\varphi}_f = \varphi_k$ for $\varphi \in \{u, v, w, \rho\}$, and $\tilde{p}_f = p_f$.

3. When the flow $F = \tilde{\rho}\tilde{\vec{u}}\vec{S}$ is calculated on the interface boundaries $\tilde{\rho} = 0.5(\rho_f + \rho_k)$, $\tilde{\vec{u}} = 0.5(\vec{u}_f + \vec{u}_k)$.

Note that in order to increase the accuracy of interpolation of quantities on the interaction interfaces, the model should be prepared subject to the fact that the cells of overlapping grids in the vicinity of the interface should not differ much in the scale (the larger is the scale difference, the greater is the approximation error). In construction of interpolation pattern, some cells of the common mesh are declared non-computational. The calculation of the flows and the recalculation of the field values should be carried out only on the faces and in the cells that are declared computational at the given time moment. Since all the grids are merged into one mesh, then at the stage of recalculation of the fields, the common matrix of the system of linear equations is solved for all cells of the common mesh. For cells declared non-computational, unity is set in the diagonal entries of the matrix and the value from the previous time step (or iteration) is set in the entries in the right-hand part.

2.2. Equations of Motion of Fluid and Allowance for Motion of Objects

Since the independent grids (there may be several of them) built for individual elements of the computational domain can be in motion and, in general, can be distorted, this should be taken into account in writing down the Navier–Stokes equations for conservatism and correct allowance for flows. Now we will consider this question in more detail.

The system of Navier–Stokes equations for calculation of unsteady three-dimensional flows of viscous incompressible gas has the following form:

$$\begin{cases} \dfrac{\partial \rho}{\partial t} + \operatorname{div}(\rho \vec{u}) = 0, \\ \dfrac{\partial (\rho \vec{u})}{\partial t} + \operatorname{div}(\rho \vec{u} \otimes \vec{u}) = -\nabla p + \operatorname{div} T + \rho \vec{g}, \end{cases} \tag{1}$$

where ρ, $\vec{u}$, p, and t are the density, velocity, pressure, and time, respectively, T is the viscous stress tensor, and $\vec{g}$ is the gravity acceleration vector;

$$T_{ij} = \mu\left(2S_{ij} - \delta_{ij}\frac{2}{3}\operatorname{div}\vec{u}\right), \qquad S_{ij} = \frac{1}{2}\left(\frac{\partial u_i}{\partial x_j} + \frac{\partial u_j}{\partial x_i}\right), \quad i,j = 1,2,3,$$

where μ is the laminar viscosity.

Solving this system numerically and applying the method of overset grids, one should perform integration of the basic equations of the system with allowance for the identity equation that reflects the movement of the grid faces and the possibility of change in the control volume:

$$\frac{\partial}{\partial t}\int\limits_{\Omega(t)} \varphi\, dV = \int\limits_{\Omega(t)} \frac{\partial \varphi}{\partial t}\, dV + \int\limits_{\partial\Omega(t)} \varphi(\dot{x}\cdot\vec{n})\, dS, \tag{2}$$

where φ is an imaginary variable, $\dot{x}$ is the velocity of the grid faces, dV is the volume element, dS is the surface element, and $\vec{n}$ is the normal to surface.

Given this equation, in application of the finite volume method [20], system (1) will take into account the motion of the grid elements in the integral form:

$$\begin{cases} \dfrac{\partial}{\partial t}\displaystyle\int\limits_{\Omega(t)} \rho\, dV + \int\limits_{\partial\Omega(t)} \rho(\vec{u}\cdot\vec{n})\, dS - \int\limits_{\partial\Omega(t)} \rho(\dot{x}\cdot\vec{n})\, dS = 0, \\ \dfrac{\partial}{\partial t}\displaystyle\int\limits_{\Omega(t)} \rho\vec{u}\, dV + \int\limits_{\partial\Omega(t)} \rho\vec{u}(\vec{u}\cdot\vec{n})\, dS - \int\limits_{\partial\Omega(t)} \rho\vec{u}(\dot{x}\cdot\vec{n})\, dS = -\displaystyle\int\limits_{\Omega} \nabla p\, dV + \int\limits_{\partial\Omega} (T\cdot\vec{n})\, dS. \end{cases} \tag{3}$$

The term $\frac{\partial}{\partial t}\int\limits_{\Omega(t)} \rho\varphi\, dV$ ($\varphi \in \{1,u,v,w\}$) reflects both variation in the conservative variables in time and the rate of change in the control volume. The resulting system of equations automatically takes into account the motion of the grid via the standard convective flow written in relative velocities $\tilde{F} = \rho\big((\vec{u}-\dot{x})\cdot\vec{n}\big)\, dS$. It should be noted here that for distorted control volumes, the conditions of geometric conservatism must be satisfied [21]:

$$\frac{\partial V}{\partial t} = \sum_f (\dot{x}\cdot\vec{n})\, dS_f. \tag{4}$$

The summation is performed over the faces f of the control volume.

Motion of bodies in fluid is described using a model of solid [22]. This model enables calculations with objects that move under the action of both external forces and forces determined by the fluid–body system itself. In particular, the body motion under the action of hydroaerodynamic forces and momenta created by them is taken into account. Such forces can introduce instability, especially in the absence of steady-state flow field, which shows itself in the instability of the iterative process of finding a solution and leads to appearance of non-physical oscillations. They are suppressed using a smoothing procedure, implemented as under-relaxation for the acting forces:

$$\vec{F}_{\text{int}} = (1-\gamma)\vec{F}^{n-1}_{\text{int}} + \gamma\vec{F}^{n}_{\text{int}}, \tag{5}$$

where $0 \le \gamma \le 1$ is the relaxation coefficient, $\vec{F}_{\text{int}}$ are the hydrodynamic forces, and n is the number of step in time.

To describe free-surface multiphase flows, system of equations (1) should be supplemented with a transport equation for the volume fractions of each phase α_k (k is the substance index)

$$\frac{\partial \alpha_k}{\partial t} + \vec{u}\nabla\alpha_k = 0. \quad (6)$$

The resulting system of equations is solved by the completely implicit VOF method [23]. In this case, free-surface flows are described using the VOF method with a high-resolution compression scheme. Simulation of incompressible multiphase flows is associated with additional difficulties because of the presence of discontinuous density field in the field of gravity. If gravity field is non-uniform because of non-uniform density field, it is necessary to correctly take into account the hydrostatic pressure gradient, especially in regions of discontinuous density field, in order to eliminate oscillations in the velocity field. In [24], to ensure the equilibrium of the force of gravity and the pressure gradient in the case of medium at rest, an algorithm was suggested based on replacing the pressure gradient in the equation of motion with its modification, which takes into account the action of the force of gravity. This modification was also applied in the algorithm SIMPLE for calculating the pressure gradient with allowance for the external gravity in the momentum conservation equation in the multiphase case. Using the chimera method to take into account all the described features of motion of bodies in viscous incompressible fluid, one will able to solve almost any problem rather accurately.

The described methods and models are implemented in the software package LOGOS. The software package LOGOS is designed to solve adjoint three-dimensional problems of convective heat and mass transfer, aerodynamics, and hydrodynamics on parallel computers [14, 25]. The software package LOGOS successfully passed the verification and showed quite good results on a series of various hydrodynamic problems [26, 27], including propagation of gravitational waves on a free surface (tsunami) [28, 29] and technical problems [30]. Calculations using highly parallel computing systems are accelerated by the multigrid method [25].

3. NUMERICAL CALCULATIONS

3.1. Plane Problem of Motion of Cylinder in Fluid

The presented method is verified on the problem of plane flow of viscous incompressible fluid around a circular cylinder with formation of vortices periodically shedding from the body surface. These vortices are called “the Karman wake.”

This problem is one of the most famous and classic tests for verification of programs that simulate motion of fluid or gas. When the critical Reynolds numbers are reached (when the flow passes from the laminar regime to the turbulent one), the wake collapses. Experimental studies of this problem are presented in detail in [31]. The experiment determines the coefficient of frontal resistance of the cylinder (C_x) and the Strouhal number (St), which reflects the time period of oscillation (or breakdown) of the vortices.

A plane flow around a cylinder is usually modeled using the inverse problem solution: a stationary flow of fluid of a predetermined velocity is incident on a stationary cylinder. Here, on the contrary, we assess the forces acting on the cylinder by addressing the forward problem. Let the cylinder move in a channel filled with viscous fluid at rest. It is assumed that at the time moment $t = 0$, the velocity of the cylinder is constant and differs from 0. We consider cases corresponding to the laminar regime of motion of cylinder with Reynolds numbers (Re) 350 and 250. The cylinder diameter $d = 0.2$ m is taken as the characteristic size.

The computational overset mesh has two overlapping regions: (1) the external grid, which is a rectangle with thickness of one cell, and (2) the grid surrounding the cylinder; this grid will move with the cylinder and slide along the external grid. The total mesh size is about 103000 cells.

The boundary conditions at all external boundaries of the domain: the plane of symmetry; the cylinder is considered as an impenetrable wall with adhesion.

The modeling is carried out using a scheme of second-order accuracy in time. The convective terms in the equation of conservation of momentum can be approximated using the counterflow scheme [20]. The time step is taken variable, provided that it complies with a Courant number of 0.9. The length of the computational domain makes it possible to determine the steady-state dynamic characteristics with sufficient accuracy.

The table below shows the results of comparison of experimental values with the calculation result.

Fig. 3. Isolines of velocity vector module.

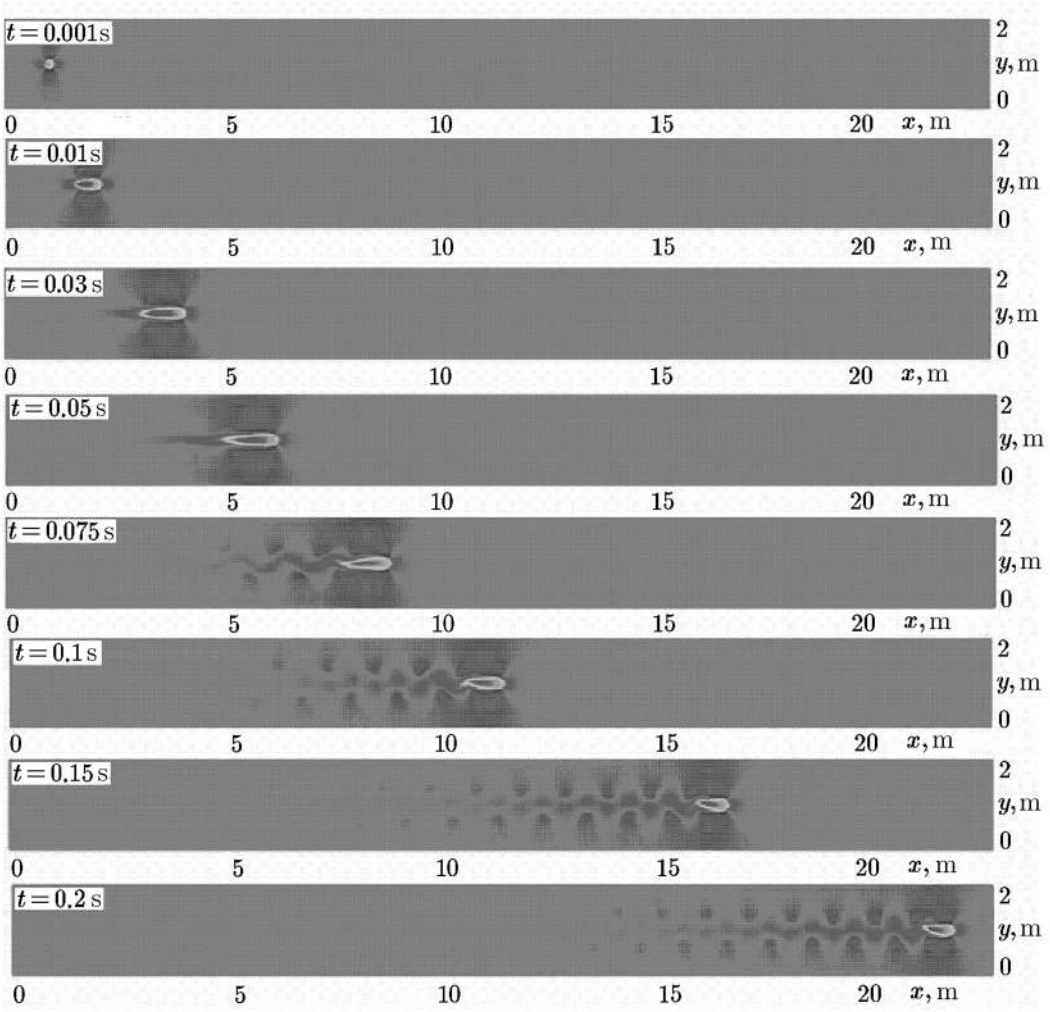

Fig. 4. Patterns of flow around cylinder at different points in time.

Results of comparison of numerical and experimental values

Reynolds number (Re)	C_x (calculation)	C_x (experiment)	Error (%)	St (calculation)	St (experiment)	Error (%)
350	1.39	1.37	1.4	0.2057	0.21	2.04
250	1.37	1.38	0.7	0.185	0.19	2.6

The results of the numerical calculations are consistent with the experimental data for both values of the Reynolds number.

Figure 3 shows a typical velocity field. Figure 4 displays flow patterns at different points in time. The presented picture corresponds to the classical description of the separation of the boundary layer in a flow around a blunt-aft body [31].

3.2. Problem of Ball Falling into Fluid

Verification of the method by modeling problems of "objects" falling into a viscous incompressible fluid can be performed on the problem of a falling ball. There are experimental data on this problem. The problem is described in detail in [32], from where the below formulation is taken.

In this problem, fall of solid ball into water is modeled. Immediately before the collision with the water surface, a ball of a radius $r = 1.27$ cm has a velocity $\bar{v} = 2.17$ m/s (Fig. 5). The water level h at the initial moment of time is 0.2 m. The computational domain is a cylinder of radius $R = 0.25$ m and height $H = 0.2255$ m.

The computational overset mesh of the modeling domain has two overlapping regions: the main grid for the entire computational domain with condensation in the area of the ball falling (it consists of arbitrary polyhedra) and the grid immediately surrounding the ball; this grid (it consists of hexagons), sliding along the main grid, will move with the ball. On the open boundary (see Fig. 5), the pressure is set; all other boundaries of the outer computational domain and the ball surface are taken as impenetrable walls without slipping. The total mesh size is about 820000 cells.

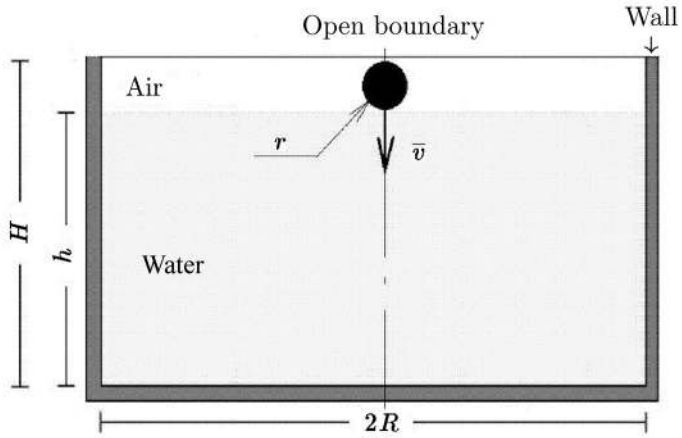

Fig. 5. Geometric parameters.

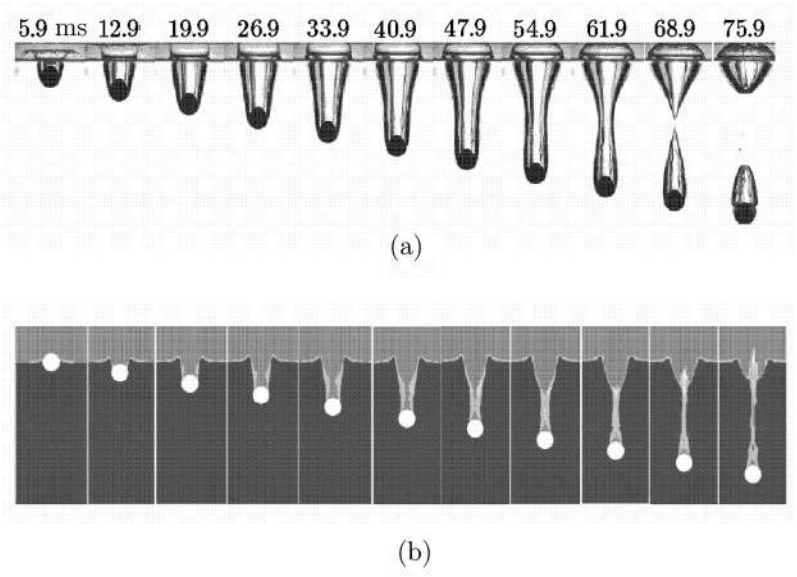

Fig. 6. Immersion of steel ball into water: (a) experimental photographs [32]; (b) numerical modeling results.

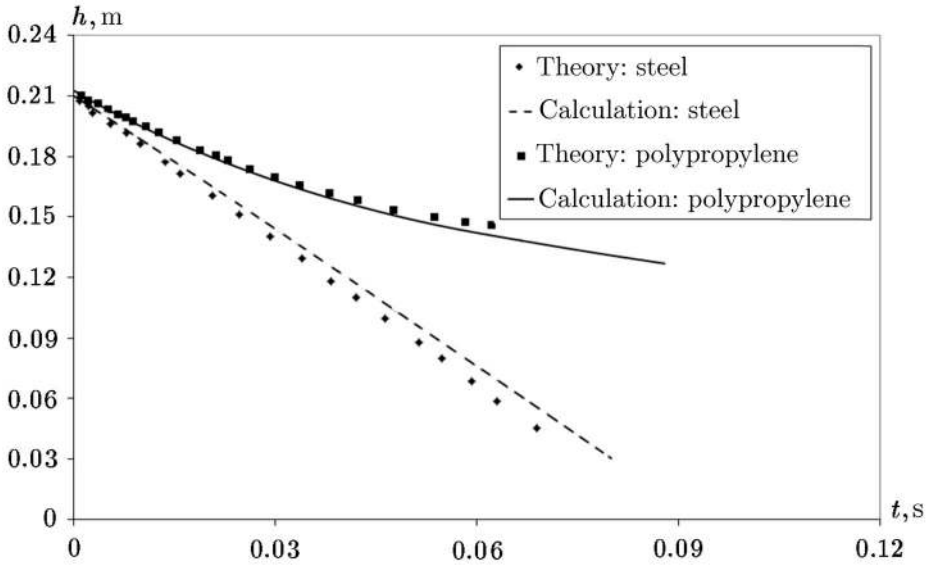

Fig. 7. Depth of immersion of ball center of mass into water vs. time.

We analyze two computational cases: in the first case, the ball material is polypropylene, whose density is 0.86 from the density of water; in the second case, it is steel with a density of 7.86 from the density of water.

Figure 6 shows the dynamics of immersion of the steel ball into water: (a) experimental photographs [32]; (b) results of numerical simulation. In Fig. 6b, the liquid phase and the air are depicted dark and gray, respectively. At the moment $t = 5.9$ ms, the ball becomes completely submerged. At the moment $t = 54.9$ ms, a cavity begins to form above the surface of the ball. By the time point $t = 68.9$ ms, the formation of the cavity ends according to the numerical simulation and is completed in the experiment. One can see good qualitative accord of the numerical and experimental results.

Figure 7 shows the depth of immersion of the ball into water versus time. Given are results for two computation cases: immersion of the steel ball and the polypropylene one. Theoretical results are presented in [32]. The accuracy of the simulation results with respect to the theoretical results is about 6%.

3.3. Flooding of Ship Model

This problem relates to the process of flooding of a reduced model of ship with damages in the bottom and in the board. The object of modeling is the compound motion of the model's hull because of buoyancy properties changing as the water flows into the hull during the flooding. In particular, considered are the interaction of the hull with the arising waves, the effect of water flowing into the ship's hull, and rotation of the ship. The results of numerical calculations are compared with the experimental data presented in paper [33].

The external domain of the modeling is a 0.5 m $\times$ 0.6 m $\times$ 0.7 m tank filled with water to a height 0.4 m. The body is a hollow parallelepiped with a rounded base and a mass of 2.15 kg. Figure 8 shows the geometrical parameters of the body in millimeters. The body dimensions with the rounding are 0.35 m $\times$ 0.17 m $\times$ 0.13 m; the wall thickness is 0.01 m (Fig. 8). Along the center line on the top of the body, there are made 6 holes of a radius 0.01 m, which are to reduce the influence of air on the sinking body (Fig. 8) [33].

Since the main cause of flooding of real ships is damage to the board or bottom, two cases (models) are considered: (A) there is an opening with a diameter of 0.09 m in the center of the bottom of the body; (B) there is a hole of a diameter 0.09 m on either side of the body.

At the initial moment, the body position is such that its bottom touches the water level (Fig. 8), and then the body begins to sink.

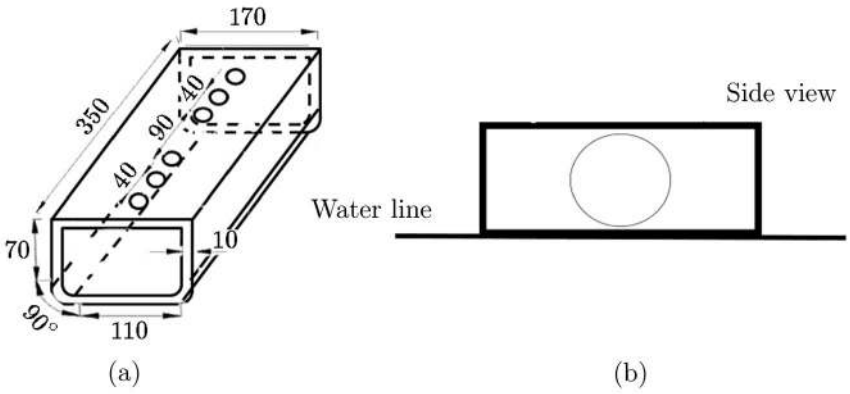

Fig. 8. Dimensions and initial position of body: (a) body dimensions; (b) initial position.

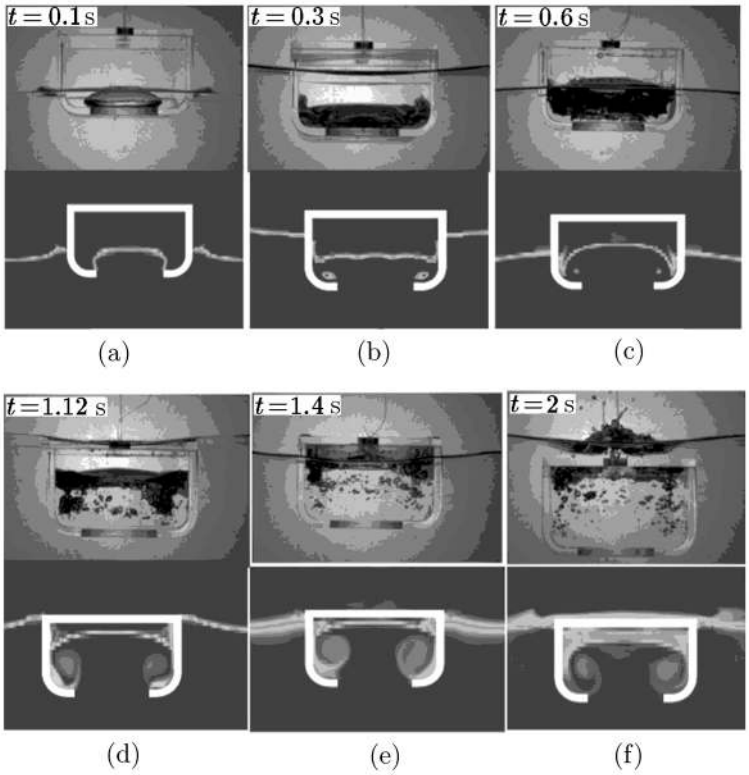

Fig. 9. Comparison of experimental photographs and numerical results (model A): (a) $t = 0.1$ s; (b) $t = 0.3$ s; (c) $t = 0.6$ s; (d) $t = 1.12$ s; (e) $t = 1.4$ s; (f) $t = 2$ s.

The overset computational mesh has two overlapping regions: (1) the external grid is a parallelepiped with the dimensions of the external tank and (2) the grid surrounding the walls of the body; this grid moves with the body and slides over the outer grid. The outer boundary of the body-coupled grid is located at a distance of 20 mm from the outer surface of the body. The entire mesh consists of hexagons; the total size is about 800000 cells.

The walls of the tank and the surface of the flooded body are considered as impenetrable rigid walls without slippage; the pressure is set on the top cover of the external tank.

The body moves under the action of external forces and torques, for which characteristics such as the body mass and inertia tensor are specified. The equations of the body motion are integrated in the global coordinate system. The result of the integration is the new coordinates of the center of gravity of the solid and the new angle of rotation. Based on the data obtained, the displacements of the nodes on the solid

surface are calculated, after which the computational grid is subjected to distortion. It is believed that the body has 6 degrees of freedom.

Considered are water and air with molecular viscosity of $\mu = 0.00101$ kg/(ms) and $\mu = 0.0000185$ kg/(ms) and density of $\rho = 998.2$ kg/m^3 and $\rho = 1.205$ kg/m^3, respectively.

The calculation results are compared with the results of the experiments described in [31]. During the experiments, photographs were taken. Figure 9 presents comparison of experimental photographs and numerical results for the model with the hole in the bottom (model A). In the display of the numerical results, the air phase is shown above, and the water phase is shown below.

At the initial moment of time, the gravity force makes the body sink into the water. In the frames shown in Fig. 9, one can see that when the water surface is above the hole in the bottom, a mushroom-shaped water column is forming inside the body. With larger depth of immersion, the buoyant force increases, and the rate of immersion decreases, falling to zero by the time $t = 0.3$ s, and the model begins to float toward the surface. The amount of water inside the model decreases until the hull rises to

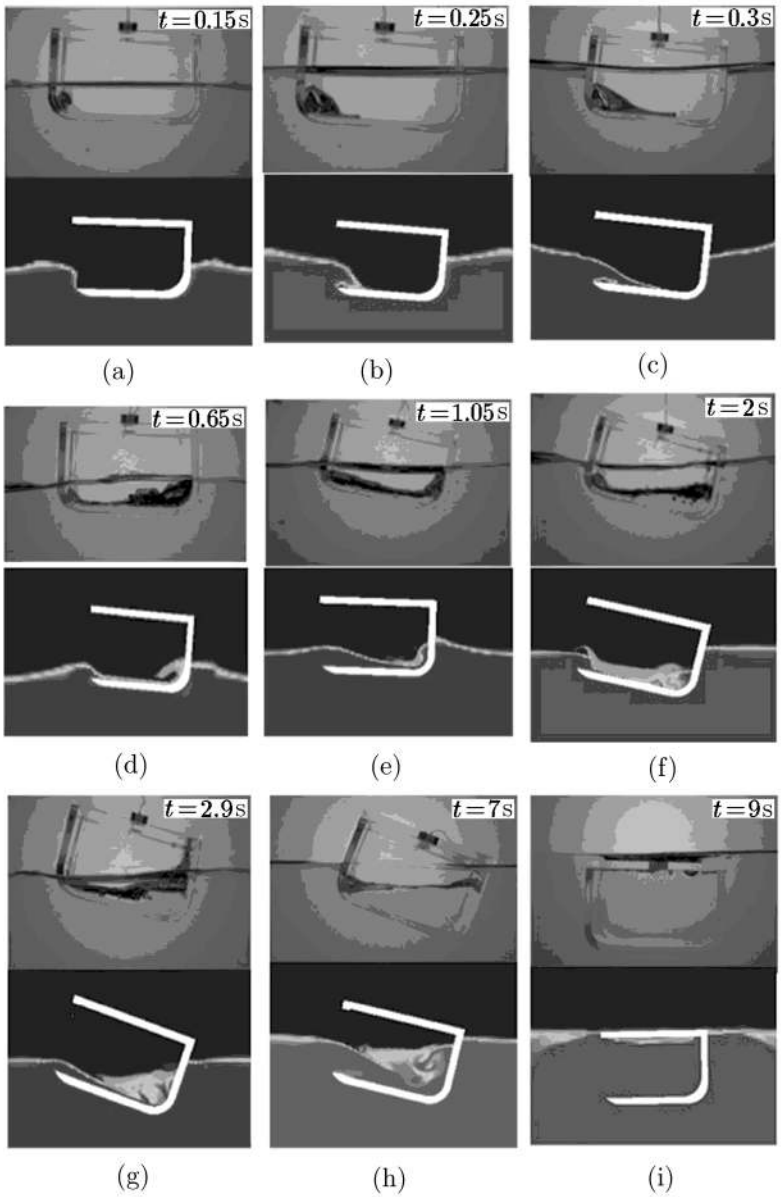

Fig. 10. Comparison of experimental photographs and numerical results (model B): (a) $t = 0.15$ s; (b) $t = 0.25$ s; (c) $t = 0.3$ s; (d) $t = 0.65$ s; (e) $t = 1.05$ s; (f) $t = 2$ s; (g) $t = 2.9$ s; (h) $t = 7$ s; (i) $t = 9$ s.

its highest point at $t = 0.6$ s. At this point, the volume of water that flowed inside is half the total internal volume of the model. Such movements of the model repeat periodically. The model is completely filled with water and finally sinks at $t = 2$ s.

Figure 10 shows a similar comparison of experimental photographs and numerical results for a model with a side opening (model B).

If the left side of the model is damaged, the center of mass shifts closer to the right side. Initially, the center of buoyancy is between the center of mass and the left side, which causes a torque that tilts the ship in the direction of the right side. From the frames presented in Fig. 10, it is clear that at $t = 0.15$ s the floating body dips in the water, and when the hole in the wall of the model gets below the water level, the water begins to flow into the body and the angle of inclination of the body increases. The deeper is the body in the water, the stronger is the emerging buoyant force, which produces the reverse acceleration. At $t = 0.25$ s, the inflowing water makes the model unstable; the sink rate decreases to zero, and the damaged side begins to float upward. Further, the ascent rate decreases with the depth of immersion. While the water flows inside the hull, the liquid rotates because of collision with the walls, which generates a torque directed to the left side of the hull. The center of buoyancy again shifts toward the right side. After the action of both restoring torques, the roll angle decreases. After repeated action of such torques, the period of oscillation becomes larger and the amplitude of body oscillations in the vertical declines. The amount of water flowing inside grows in the course of immersion and decreases in

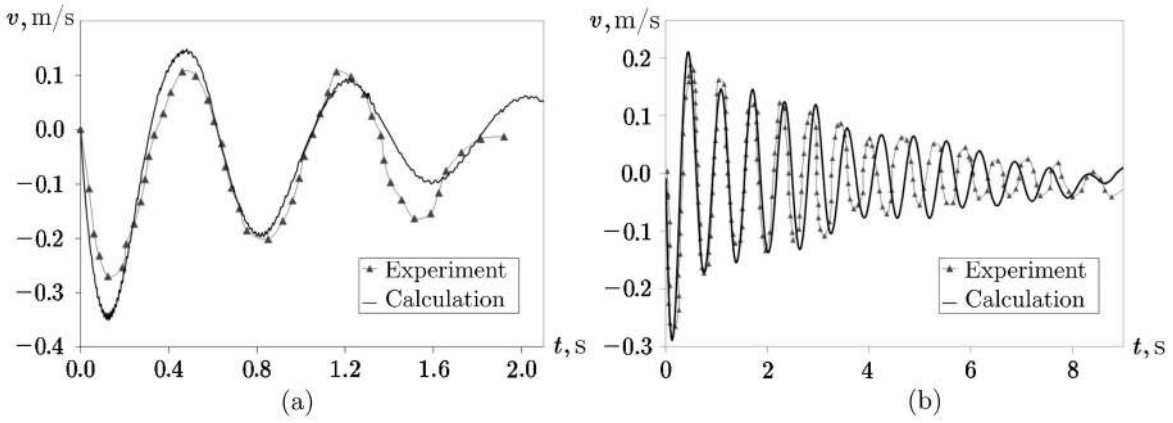

Fig. 11. Vertical component of body velocity: (a) model A; (b) model B.

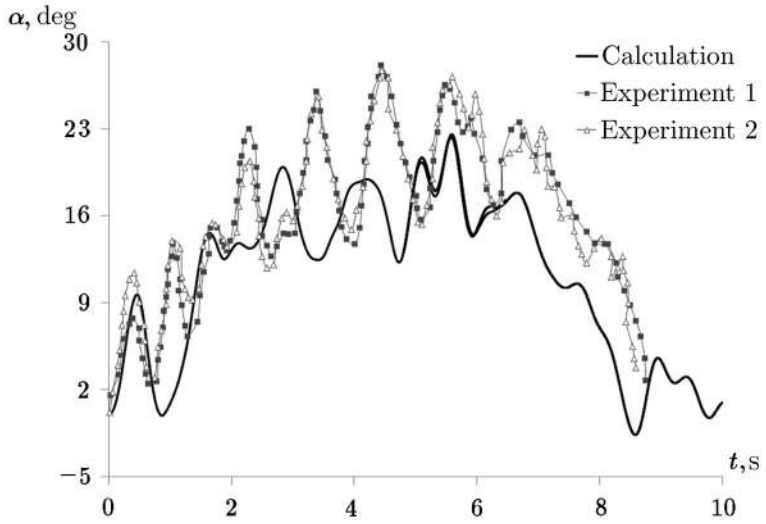

Fig. 12. Body roll angle for model with side hole.

the course of ascent. After several periods of oscillation in vertical direction, at $t = 7$ s the motion of the model becomes steady till $t = 9$ s, when the body is completely submerged.

The practical experiment yielded graphs of changes in the vertical velocity of the body (models A and B) and the angle of roll (model B). These data were compared with the results of the numerical experiment.

Figure 11 presents comparison of the experimental and calculated data on the change in the vertical component of the body velocity with time. Figure 12 shows the change in the roll angle with time for two experiments from a series, as well as numerical calculation for model B.

Comparison of the calculated and experimental data shows that at the initial stage of immersion, they are very close both qualitatively and quantitatively for the model A and the model B. This can be seen both from the frames of the phase distribution field and from the graphs (Figs. 11 and 12).

Further, at the final stage of the flooding, when the body is fully immersed in the water, one can see slower damping of the body motion oscillations in the vertical plane as compared with the experiment (model A and model B). This difference is especially noticeable for the model A, where at $t = 2$ s the experiment shows that the body is completely submerged and begins to sink, whereas the calculation data suggests that the body keeps oscillating near the surface, gradually sinking deeper and deeper under the water.

CONCLUSIONS

This paper demonstrated the possibilities of simulation of the motion of bodies in viscous incompressible fluid by the chimera technique on unstructured computational grids using the finite volume method for discretization. Particularities of such simulation in the context of the algorithm used are noted. The features of the simulation in the presence of multiphase media were taken into account. An algorithm for processing the interface faces was presented; the dual representation of interface faces as both internal faces of the computational grid and external faces for a separate geometric region was taken into account.

Solutions to the problems of cylinder motion in liquid, ball falling into liquid, and flooding of ship model obtained by the method described were presented. In all the cases, the numerical results were in good agreement with the experimental data. Further studies may involve solving problems with more complex geometry and numerical description of complex types of movements. Using unstructured meshes along with the chimera method will significantly reduce the number of subdomains in the case of complex geometries.

FUNDING

The work was performed under a state assignment in the field of scientific activity (project nos. 5.4568.2017/6.7 and 5.1246.2017/4.6) and supported by RFBR (project no. 16-01-00267), by the Council for Grants (under RF President) and State Aid of Leading Scientific Schools (grant NSh-2685.2018.5), and by the Grants Council (under RF President), grant no. MD-4874.2018.9.

REFERENCES

1. Kiris, C., Kwak, D., Rogers, S., and Chang I., Computational Approach for Probing the Flow through Artificial Heart Devices, *J. Biomech. Eng.*, 1997, vol. 119, no. 4, pp. 452–460.
2. Tahara, Y., Wilson, R., Carrica, P., and Stern, F., RANS Simulation of a Container Ship Using a Single-Phase Level-Set Method with Overset Grids and the Prognosis for Extension to a Self-Propulsion Simulator, *J. Marine Sci. Technol.*, 2006, vol. 11, no. 4, pp. 209–228.
3. Fast, P. and Shelley, M.J., A Moving Overset Grid Method for Interface Dynamics Applied to Non-Newtonian Hele-Show Flow, *J. Comput. Phys.*, 2004, vol. 195, pp. 117–142.
4. Mazhukin, V.I., Samarskii, A.A., Kastelianos, O., and Shapranov, A.V., Dynamic Adaptation Method for Non-Stationary Problems with Large Gradients, *Mat. Model.*, 1993, vol. 5, no. 4, pp. 32–56.
5. Godunov, S.K. and Prokopov, G.P., The Use of Moving Meshes in Gas-Dynamical Computations, *Comput. Math. Math. Phys.*, 1972, vol. 12, no. 2, pp. 182–195.
6. Mittal, R. and Iaccarino, G., Immersed Boundary Methods, *Ann. Rev. Fluid Mech.*, 2005, vol. 37, pp. 239–261.

7. Benek, J.A., Buning, P.G., and Steger, J.L., A 3D Chimera Grid Embedding Technique, *Proc. 7th Comput. Phys. Conf.*, Cincinnati, OH, USA, *AIAA J.*, 1985, pp. 322–331 (AIAA 85-1523); DOI:10.2514/6.1985-1523.
8. Abalakin, I.V., Zhdanova, N.S., and Kozubskaya, T.K., Implementation of the Method of Immersed Boundaries for Simulation of External Flow Problems on Unstructured Meshes, *Mat. Model.*, 2015, vol. 27, no. 10, pp. 5–20.
9. Wang, Z.J. and Parthasarathy, V., A Fully Automated Chimera Methodology for Multiple Moving Body Problems, *Int. J. Num. Meth. Fluids*, 2000, vol. 33, no. 7, pp. 919–938.
10. Lee, K.R., Park, J.H., and Kim, K.H., High-Order Interpolation Method for Overset Grid Based on Finite Volume Method, *AIAA J.*, 2011, vol. 49, no. 7, pp. 1387–1398.
11. Hahn, S., Iaccarino, G., Ananthan, S., and Baeder, D., Extension of CHIMPS for Unstructured Overset Simulation and Higher-Order Interpolation, *Proc. 19th AIAA Computational Fluid Dynamics, Fluid Dynamics and Co-Located Conf.*, San Antonio, Texas, *AIAA Paper*, 2009, pp. 299–311 (AIAA 2009-3999); DOI:10.2514/6.2009-3999.
12. Tang, H., Jones, S.C., and Sotiropoulos, F., An Overset Grid Method for 3D Unsteady Incompressible Flows, *J. Comput. Phys.*, 2003, vol. 191, no. 2, pp. 567–600.
13. Wang, Z.J. and Yang, H.Q., A Unified Conservative Zonal Interface Treatment for Arbitrarily Patched and Overlapped Grids, *32nd Aerospace Sciences Meeting and Exhibit*, Reno, NV, USA, *AIAA Paper*, 1994 (AIAA 94-0320); DOI:10.2514/6.1994-320.
14. Kozelkov, A.S., Shagaliev, R.M., Kurulin, V.V., Yalozo, A.V., and Lashkin, S.V., Investigation of Supercomputer Capabilities for the Scalable Numerical Simulation of Computational Fluid Dynamics Problems in Industrial Applications, *Comput. Math. Math. Phys.*, 2016, vol. 56, no. 8, pp. 1506–1516.
15. Pogosyan, M.A., Savel'evskikh, E.P., Shagaliev, R.M., et al., Application of Supercomputer Technologies in the Russian Aviation Industry, in *Mezhdunarodnaya entsiklopediya CALS-tekhnologii. Aviatsionno-kosmicheskoe mashinostroenie* (International Encyclopedia of CALS Technologies. Aerospace Engineering), Bratukhina, A.G., Ed., Moscow: OAO NITS ASK, 2015, pp. 49–61.
16. Marco, A., Mancini, S., Miranda, S., Scognamiglio, R., and Vitiello, L., Experimental and Numerical Hydrodynamic Analysis of a Stepped Planing Hull, *Appl. Ocean Res.*, 2017, vol. 64, pp. 135–154.
17. Usachov, A.E., Mazo, A.B., Kalinin, E.I., et al., Improving the Efficiency of Numerical Modeling of Turbulent Separated Flows by Using Hybrid Grids with Structured Multi-Scale Blocks and Unstructured Inserts, *Trudy MAI*, 2018, no. 99.
18. Zhang, X., Computation of Viscous Incompressible Flow Using Pressure Correction Method on Unstructured Chimera Grid, *Int. J. Comput. Fluid Dyn.*, 2006, vol. 20, no. 9, pp. 637–650.
19. Deryugin, Yu.N., Sarazov, A.V., and Zhuchkov, R.N., Features of Construction of Calculation Technique on Chimera Grids for Unstructured Grids, *Mat. Model.*, 2017, vol. 29, no. 2, pp. 106–118.
20. Ferziger, J.H. and Peric, M., *Computational Method for Fluid Dynamics*, New York: Springer-Verlag, 2002.
21. Farhat, C., Geuzaine, Ph., and Grandmonty, C., The Discrete Geometric Conservation Law and the Nonlinear Stability of ALE Schemes for the Solution of Flow Problems on Moving Grids, *J. Comput. Phys.*, 2001, vol. 174, pp. 669–694.
22. Borisov, A.V. and Mamaev, I.S., *Dinamika tverdogo tela. Regulyarnaya i khaoticheskaya dinamika* (Dynamics of Solid Body. Regular and Chaotic Dynamics), Izhevsk, 2001.
23. Kozelkov, A.S., Meleshkina, D.P., Kurkin, A.A., et al., Completely Implicit Method for Solving Navier–Stokes Equations for Calculating Multiphase Free-Surface Flows, *Vych. Tekhnol.*, 2016, vol. 21, no. 5, pp. 54–76.
24. Efremov, V.R., Kozelkov, A.S., Kornev, A.V., Kurkin, A.A., Kurulin, V.V., Strelets, D.Y., and Tarasova, N.V., Method for Taking into Account Gravity in Free-Surface Flow Simulation, *Comput. Math. Math. Phys.*, 2017, vol. 57, no. 10, pp. 1720–1733.
25. Volkov, K.N., Deryugin, Yu.N., Emel'yanov, V.N., et al., *Metody uskoreniya gazodinamicheskikh raschetov na nestrukturirovannykh setkakh* (Methods of Accelerating Gas-Dynamic Calculations on Unstructured Grids), Moscow: Fizmatlit, 2013.
26. Kozelkov, A.S., Kurulin, V.V., Tyatyushkina, E.S., Kurkin, A.A., Legchanov, M.A., and Tsibereva, Y.A., Investigation of the Application of RANS Turbulence Models to the Calculation of Nonisothermal Low-Prandtl-Number Flows, *Fluid Dyn.*, 2015, vol. 50, no. 4, pp. 501–513.
27. Kozelkov, A.S., Kurkin, A.A., Krutyakova, O.L., Kurulin, V.V., and Tyatyushkina, E.S., Zonal RANS–LES Approach Based on an Algebraic Reynolds Stress Model, *Fluid Dyn.*, 2015, vol. 50, no. 5, pp. 621–628.
28. Kozelkov, A.S., Kurkin, A.A., Pelinovsky, E.N., Kurulin, V.V., and Tyatyushkina, E.S., Numerical Modeling of the 2013 Meteorite Entry in Lake Chebarkul, Russia, *Nat. Hazards Earth Syst. Sci.*, 2017, vol. 17, pp. 671–683.

29. Kozelkov, A.S., Kurkin, A.A., Pelinovsky, E.N., et al. Landslide-Type Tsunami Modeling Based on the Navier–Stokes Equations, *Sci. Tsunami Hazards*, 2016, vol. 35, no. 3, pp. 106–144.
30. Betelin, V.B., Shagaliev, R.M., Aksenov, S.V., et al., Mathematical Simulation of Hydrogen–Oxygen Combustion in Rocket Engines Using LOGOS Code, *Acta Astronautica*, 2014, vol. 96, no. 1, pp. 53–64.
31. Schlichting, H., *Grenzschicht-Theorie*, Karlsruhe: G. Braun, 1951.
32. Aristoff, J.M., Truscott, T.T., Techet, A.H., and Bush, J.W.M., The Water Entry of Decelerating Spheres, *Phys. Fluids*, 2010, vol. 22, iss. 3 (no. 032102); DOI:10.1063/1.3309454.
33. Zhang, A., Cao X., Ming, F., and Zhang, Z., Investigation on a Damaged Ship Model Sinking into Water Based on Three-Dimensional SPH Method, *Appl. Ocean Res*., 2013, vol. 42, pp. 24–31.